Automatic Generation Control-based Charging/Discharging Strategy for EV fleets to Enhance the Stability of a Vehicle-To-Weak Grid System

Majid Mehrasa[1], Mehrdad Gholami[1,2], Reza Razi[3], Khaled Hajar[3], Antoine Labonne[1], Ahmad Hably[3], and Seddik Bacha[1]
[1]Univ. Grenoble Alpes, CNRS, Grenoble INP, G2ELAB, 38000 Grenoble, France
[2]Faculty of engineering, University of Kurdistan, Sanandaj, Iran
[3]Univ. Grenoble Alpes, CNRS, Grenoble INP, GIPSA-Lab, 38000 Grenoble, France
majid.mehrasa@g2elab.grenoble-inp.fr

Acknowledgements

This work has been supported by the aVEnir project of the PIA operated by ADEME.

Keywords

«EVs Fleet», «Automatic Generation Control», «Weak Power Grid», «Balancing Power», «Frequency Control».

Abstract

In this paper, an automatic generation control (AGC)-based charging/discharging strategy is proposed for EV fleets to augment the stability of a weak power grid (WPG). The Vehicle-to-Weak Grid (V2WG) system under study is indeed a two-area microgrid including WPG, two EVs stations, PV units and loads. Firstly, the balancing power relation for three operating modes including no change mode, load increment and PV increment are comprehensively investigated. In doing so, a power sharing algorithm for each active EV is proposed to contribute to the WPG frequency deviation compensation. Then, AGC is developed for each area to attain the related angular frequency errors which are aimed to provide the tie-line power error needed for the dynamical frequency variation compensation using the appropriate EVs action. Moreover, the proposed strategy coefficients are analyzed to understand how much they can impact the stability margin of the system angular frequency errors. The simulation results in MATLAB/SIMULINK environment validate the ability of the proposed strategy-based EV fleets at providing a stable WPG under the increment of both load and PV units.

Introduction

Electric Vehicles (EVs) have continuously attracted the researcher's attention to be developed for Vehicle-to-Grid (V2G) applications using the bidirectional power transfer achieved from huge value of the battery energy of the Aggregated EVs [1-4]. Aggregated EVs can take the role of power grid frequency stabilizer while a high penetration of renewable energy resources (RERs) integrates into power grid or a large amount of load variations occurs [5-7]. Different challenges regarding EVs charging strategies have been discussed in recent years such as parking fleet scenario with modular converters [8], revenue assessment with wear cost model [9], PVs at the electric mobility's service [10-11], and different PEV parking scenarios [12]. But, the frequency vulnerability is an interesting challenge that is boosted in the presence of a weak power grid wherein much more accurate smart charging /discharging strategies must be designed for EVs by taking into account the required power for the appropriate frequency deviation compensation [13]. The appropriate compensation means both fast and accurate reactions achieved through i) the identification of EV rated power, ii) coordination between the EVs power sharing and the frequency deviation, and iii) maximum utilization of EV charging stations, and so on.

The secondary frequency control loop has been regarded as a target for researchers to be fortified by enhancing the EVs charging participation against power grid instabilities. To this end, the references [14], [15] and [16] have dealt with the grid secondary frequency control using respectively optimized fuzzy technique, mixed integer linear programming (MILP) and aggregator-based hierarchical strategy.

The secondary frequency control loop may be exposed to a stability uncertainty made by the aggregation dynamics and its delays. For this case, Ref [17] proposed an integration for the effects of heterogeneous delay and ascertained the sequential impact procedure for aggregation delays. On the other hand, some criteria in Ref [18] were taken into account such as various charging profiles, the SOC of EVs, and the numbers of EVs to enable a primary frequency loop aiming to attain flexible bidirectional power flow. The cooperation between wind system and EVs for completing the primary frequency loop of a microgrid was made by using small-signal analysis to establish frequency regulation strategy and droop or virtual inertia [19]. In the frequency regulation process, it has challenged a coordination between the power sharing control system and the SOC of EV batteries. This challenge was investigated through Ref [20] based on assigning the uncertain dispatch inside the control loop with no information regarding detailed EV charging/discharging in which the adjustment task was completed within the frequency control capacity of EVs. Using an aggregator-based coordination strategy, Ref [21] focused on assessment of a large number of EVs to fulfill the centralized supplementary frequency adjustment of the interlinked power systems. Also, the time delay of power systems was taken into account in [22] based on static output feedback frequency stabilization to provide the coordinate charge control for EVs. Among various control strategies incorporated by the charging schemes of EVs for the frequency control process, automatic generation control (AGC) has been also paid attention in recent literatures [23-24]. Several myopic/non-myopic-based real-time scheduling schemes were designed in [25] to provide suitable charging/discharging method of EVs fleet based on following out the signals generated through AGC. A wide-area virtual power plant (WVPP) was made in [26] including wind farms (WFs), photovoltaic units (PVs), and EVs wherein AGC was employed to noticeably guarantee the system response acceleration and the regulation cost mitigation due to unbalanced power mismatches between generation side and demand side. In Ref [27], the optimization factors including the performance-based compensation schedule, the AGC signals, and the EVs arrival and departure times were taken into account for solving a frequency regulation capacity scheduling problem to appoint the EV frequency adjustment service. In order to achieve the optimal solutions for a multi-area energy system, the DQ algorithm and double learning were utilized for the AGC-based frequency control under contributory obligation of battery energy storages, EVs and traditional power plants [28].

In this paper, a charging/discharging strategy is proposed for EV fleets to provide stable voltage for WPG while the PV units and interconnected loads are abruptly increased. To this end, a two-area microgrid is considered which consists of a WPG, two EV stations, PV units and loads. The proposed method is made through a pervasive balancing power and an AGC assigned for each area. The paper is organized as follows. The first section is allotted to the introduction. In section II, the considered two-area mcirogrid is described. The pervasive balancing power is discussed in section III. Section IV concentrates on the proposed AGC-based strategy. Simulation results and conclusion are respectively presented in Sections V and VI.

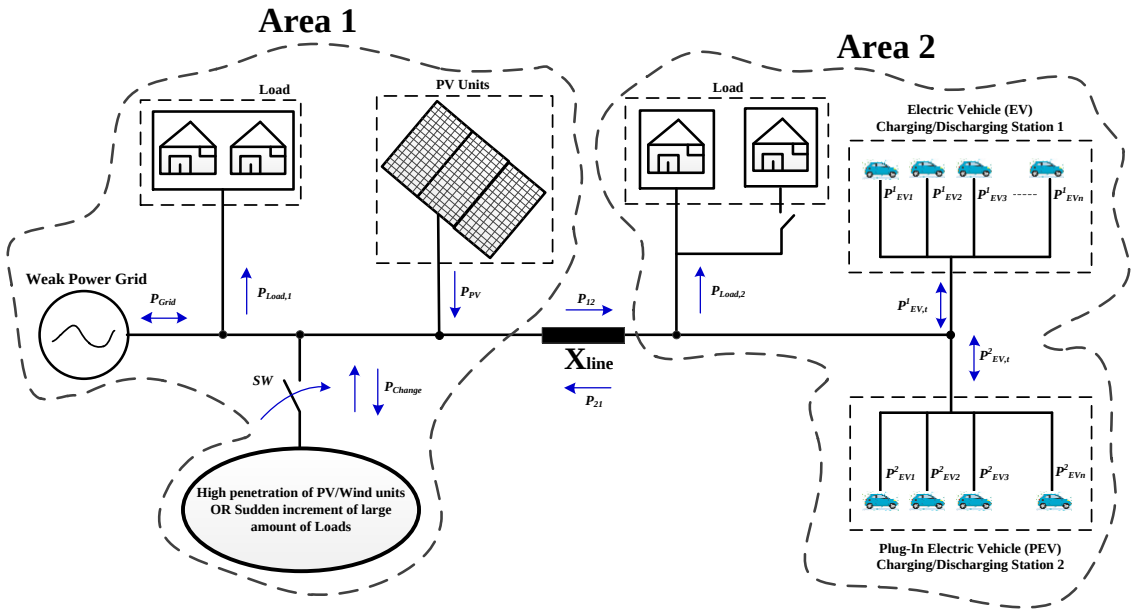

Fig. 1: The proposed V2WG-based two-area System.

Description of the considered two-area system

The two-area microgrid under study in this paper is displayed in Fig. 1. The WPG is placed within the first area and also the high-penetration renewable energies or a large amount of abrupt load variation will happen in this area. In addition, the PV units and load are included in the first area as well. As it can be seen from Fig. 1, two EVs charging/discharging stations are appointed in the second area that should be under a control process for an appropriate adjustment of WPG frequency. These EV fleets are also controlled to supply the loads in the second area. Two areas are interconnected through the inductance X_{line}.

Pervasive balancing power

The power in the microgrid shown in Fig. 1 must be controlled to enable a fast and precise frequency response for the WPG against high penetration of PV units or sudden increment of a large amount of loads. The power balance is the mandatory relation that should be taken into account by the proposed strategy. Based on Fig. 1, the balancing relation is acquired through the equation (1),

$$P_{Load} = P_{Grid} + P_{PV} + P_{EV,t} + (SW)(-1)^k P_{Change} + P_{X_{line}} \quad (1)$$

In the relation (1), when there is a new connection of PV units or Load, the *SW* (that acts as a switch) gets 1 and otherwise *SW*=0. Also, *k* is equalized to 1 and 2 for load connection and PV unit connection, respectively. The load power in (1) is achieved through $P_{Load}=P_{Load1}+P_{Load2}$. The P_{Xline} is the power due to the inductance X_{line} that has a key role at regulating the WPG frequency. It is realized from Fig. 1 that the total power of both EV charging/discharging stations is achieved through $P_{EV,t}=P^1_{EV,t}+P^2_{EV,t}$. The total power of each station is dependent on the number of the existing EVs as well as the instantaneous power of each EV. It is assumed that the first and second station respectively has "*m*" and "*n*" EVs. By noticing Fig. 1, the total power of EVs charging/discharging stations can meet,

$$P_{EV,t} = \sum_{j=1}^{n} P^1_{EV,j} + \sum_{j=1}^{m} P^2_{EV,j} \quad (2)$$

Using the relations (1) and (2), the total EVs power can be stated based on the power of load, the grid, PV, the inductance power and the additional load/PV,

$$\sum_{j=1}^{n} P^1_{EV,j} + \sum_{j=1}^{m} P^2_{EV,j} = P_{Load} - P_{Grid} - P_{PV} - (SW)(-1)^k P_{Change} - P_{X_{line}} \quad (3)$$

Three operating conditions are considered for the balancing power relation (3). These conditions are explained as the following to reach the most effective Frequency Regulation Strategy (FRS).

The microgrid with no PV/load increment

The first operating condition is fulfilled by *SW*=0. It means that there is no the PV/load increment. In this condition, while accurate prediction is accomplished for PV and load, the WPG encounters relatively a zero frequency alteration. Thus, the first and second stations tend to meet the following total power,

$$\sum_{j=1}^{n} P^1_{EV,j} = \alpha\left(P_{Load} - P_{Grid} - P_{PV} - P_{X_{line}}\right) \quad (4)$$

$$\sum_{j=1}^{m} P^2_{EV,j} = (1-\alpha)\left(P_{Load} - P_{Grid} - P_{PV} - P_{X_{line}}\right) \quad (5)$$

The coefficient α is determined with respect to the total existing rated power of each station wherein the higher power share belongs to the station with higher instantaneous power. As a consequence, the proposed charging/discharging method should enforce the EV of each station to be charged/discharged according to the relations (6) and (7),

$$P^1_{EV,x} = \beta^1_x\left[\alpha\left(P_{Load} - P_{Grid} - P_{PV} - P_{X_{line}}\right)\right] \quad (6)$$

$$P^2_{EV,y} = \beta^2_y\left[(1-\alpha)\left(P_{Load} - P_{Grid} - P_{PV} - P_{X_{line}}\right)\right] \quad (7)$$

Where x=1, …, n and y=1, …, m. The coefficients $\beta^1{}_x$ and $\beta^1{}_y$ are adjusted by taking the EV specifications into account such as the rated power and the difference between the arrival and departure time. In addition, the relations $\sum_{x=1}^{n}\beta_x^1=1$ and $\sum_{y=1}^{m}\beta_y^1=1$ must be assured.

The microgrid with PV/load increment

High PV penetration and load increment are other challenges of WPG frequency that can be dealt with by the EV charging/discharging stations. Based on the relation (3), high PV penetration occurs when SW=1 and k=2 leading to,

$$\sum_{j=1}^{n}P_{EV,j}^{1}+\sum_{j=1}^{m}P_{EV,j}^{2}=P_{Load}-P_{Grid}-\left(P_{PV}+P_{Change}^{PV}\right)-P_{X_{line}} \tag{8}$$

Where $P^{PV}{}_{Change}$ is the power injected from the PV units which are abruptly integrated into the WPG at a specified time. Since the PV units inject power into the WPG, it is highly probable that most EVs in both stations proceed at charging mode. To this end, the following inequality must be satisfied,

$$P_{PV}+P_{Change}^{PV}>\left[P_{Load}-P_{Grid}-P_{X_{line}}\right] \tag{9}$$

The inequality (9) depends on the load power and subsequently the power grid can be chosen as a constant value or within limited constraints because of the sensibility of WPG frequency. The load connection is taken into account through SW=1 and k=1 wherein the relation (3) can meet,

$$\sum_{j=1}^{n}P_{EV,j}^{1}+\sum_{j=1}^{m}P_{EV,j}^{2}=\left(P_{Load}+P_{Change}^{Load}\right)-P_{Grid}-P_{PV}-P_{X_{line}} \tag{10}$$

In equation (10), the $P^{Load}{}_{Change}$ is the additional load interconnecting with the WPG at a specified time. For general discussion, the load variation in the second area also is involved with the $P^{Load}{}_{Change}$ having approximately the same impact on the WPG. When the additional load is appeared, most EVs can be presumed to be discharged. This condition is made through (11),

$$P_{Load}+P_{Change}^{Load}>P_{Grid}+P_{PV}+P_{X_{line}} \tag{11}$$

In fact, the inequalities (9) and (11) can be employed to identify the charging or discharging states of two EVs fleet in various operating conditions.

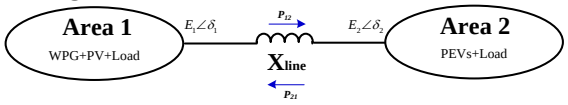

Fig. 2: The net tie-line power representation for a two-area system.

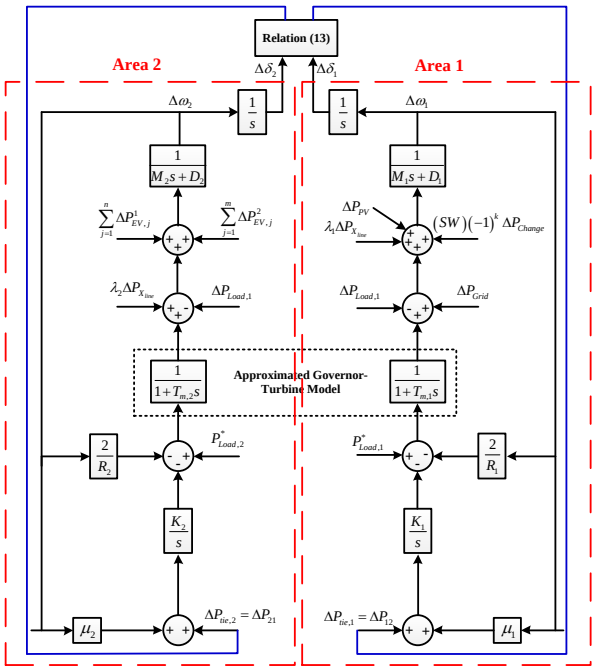

Fig. 3: The proposed AGC-based control.

Proposed AGC-based strategy

Each area in the proposed V2WG-based two-area microgrid shown in Fig. 1 is regarded as the independent generation unit that is responsible for reaching desired value for the frequency in its own area. In doing so, Automatic Generation Control (AGC) is allotted to each area commensurate with compensating the WPG frequency deviations and fulfilling effective charging/discharging procedures for EV stations. Before starting the AGC design for each area, it is worth investigating on the net tie-line power error ΔP_{12}=-ΔP_{21} and the relation between the tie-line power and the area frequency. The tie-line power of a two-area system with the inductance interface that has the specifications according to Fig. 2 can be written,

$$P_{12} = \frac{E_1 E_2}{X_{line}} \sin(\delta_1 - \delta_2) \tag{12}$$

In relation (12), $E_{1(2)}$ and $\delta_{1(2)}$ are the voltage characteristics of the control areas named the voltage magnitude and the voltage angle, respectively. The small-signal linearization is exerted to (12) around the equilibrium points of P^*_{12} and $\delta^*_{1(2)}$ with the approximation $\Delta E_{1(2)}$=0. This linearization results in the relation between the frequency and the tie-line power error according to (13),

$$\Delta P_{12} = \left(X_{line}\right)^{-1} \left[E_1^* E_2^* \cos\left(\delta_1^* - \delta_2^*\right) \times \int \left(\Delta\omega_1 - \Delta\omega_2\right) dt \right] \tag{13}$$

The relation (13) determines that the tie-line power error has a key role at the instantaneous calculation of the area frequency. The following sub-sections concentrate on the frequency AGC-based control design for the areas.

The control design details for the area i^{th}

Each area is composed of various parts that can contribute to the frequency adjustment process as much as possible. To deeply understand this issue, it is mandatory to possess the angular frequency error formulation in the areas i^{th} based on the AGC that is just as,

$$\Delta\omega_i = \left(M_i s + D_i\right)^{-1} \left(\Delta P_{m,i} - \Delta P_{L,i} - \Delta P_{tie,i}\right) \tag{14}$$

Where M_i and D_i are the equivalent inertia and load-damping constant, respectively. The tie-line power error $\Delta P_{tie,i}$ is another variable that can impact on the frequency error of the area i^{th}. On the other hand, the variable $\Delta P_{m,i}$ in (14) is the input mechanical power that can be detailed as follows,

$$\Delta P_{m,i} = \left(1 + T_{m,i} s\right)^{-1} \left(P^*_{Load,i} - 2\left(R_i\right)^{-1} \Delta\omega_i - \frac{K_i}{s} ACE_i \right) \tag{15}$$

It should be noticed that R_i and K_i are the droop and integral controller coefficients, respectively. In addition, ACE_i is named as the Area Control Error (ACE) dedicated to the area i^{th}. The ACE_i is defined as stated in (16) to keep the frequency and power interchanges at the scheduled values in which μ_i is the ACE i^{th} frequency response characteristic,

$$ACE_i = \mu_i \Delta\omega_i + \Delta P_{tie,i} \tag{16}$$

As it can be realized from Fig. 1, the first area consists of WPG, PV units, and load that is also exposed to both high penetration of PV units and abrupt increment of load. It can be concluded that the angular frequency error of the first area is equiponderated with,

$$\Delta\omega_1 = \left(M_1 s + D_1\right)^{-1} \begin{pmatrix} \Delta P_{m,1} - \Delta P_{Load,1} + \Delta P_{Grid} \\ + \Delta P_{PV} + \left(SW\right)\left(-1\right)^k \Delta P_{Change} + \lambda_1 \Delta P_{X_{line}} \end{pmatrix} \tag{17}$$

The sharing factor of the inductance power for the first area is the coefficient λ_1. On the other hand, the two EVs charging/discharging stations are situated in the second area and have a vital role at the frequency regulation process. The angular frequency error in (18) is presented for the second area,

$$\Delta\omega_2 = \left(M_2 s + D_2\right)^{-1} \begin{pmatrix} \Delta P_{m,2} - \Delta P_{Load,2} \\ + \sum_{j=1}^{n} \Delta P^1_{EV,j} + \sum_{j=1}^{m} \Delta P^2_{EV,j} + \lambda_2 \Delta P_{X_{line}} \end{pmatrix} \tag{18}$$

As it was mentioned, λ_2 denotes the sharing factor of the inductance power for the second area. The sharing factors of the inductance power must be proportionate to the frequency deviation of each area.

The proposed AGC-based control for completing the EVs charging/discharging proceeding in the system under study is illustrated in Fig. 3.

The assessment of the AGC-based controller coefficients

The proposed AGC-based charging/discharging strategy consists of different coefficients including {M_i, D_i, $T_{m,i}$, R_i, K_i, μ_i} that all need to be appropriately selected. To this end, the relations (15) and (16) are substituted into (14) resulting in,

$$\Delta\omega_i = \left(M_i s + D_i\right)^{-1}\left(\left(1+T_{m,i}s\right)^{-1}\begin{pmatrix} P^*_{Load,i} - 2\left(R_i\right)^{-1}\Delta\omega_i \\ -\dfrac{K_i}{s}\left(\mu_i\Delta\omega_i + \Delta P_{tie,i}\right)\end{pmatrix} - \Delta P_{L,i} - \Delta P_{tie,i}\right) \tag{19}$$

And finally the angular frequency error of the area i^{th} is attained after some mathematical simplifications according to (20),

$$\Delta\omega_i = H_{Load,\mathrm{Re}f}(s)P^*_{Load,i} + H_{tie,i}(s)\Delta P_{tie,i} + H_{L,i}(s)\Delta P_{L,i} \tag{20}$$

The angular frequency error consists of the transfer functions that are a consequence of the reference load power, tie-line power error, and load power error. The transfer functions in (20) are achieved using (21),

$$\begin{aligned} &H_{Load,\mathrm{Re}f}(s) = s/\Delta_i, H_{tie,i}(s) = \left(T_{m,i}s^2 + s - K_i\right)/\Delta_i \\ &H_{L,i}(s) = -\left(T_{m,i}s^2 + s\right)/\Delta_i \\ &\Delta_i = \left(M_i T_{m,i}s^3 + \left(D_i T_{m,i} + M_i\right)s^2 + \left(2\left(R_i\right)^{-1} + D_i\right)s + K_i\mu_i\right) \end{aligned} \tag{21}$$

The steady-state response of the angular frequency error is dependent on the transfer function $H_{tie,i}(s)$ while t $\rightarrow \infty$ leading to,

$$\Delta\omega_i(s=0) = \left(\mu_i\right)^{-1}\Delta P_{tie,i} \tag{22}$$

Based on (22), the frequency response characteristic and tie-line power error can impact the steady-state response of WPG frequency at the same time. The Nyquist diagrams are plotted in Fig. 4 to determine the contributions of AGC-based controller coefficients at the stability margin expansion. In Fig. 4(a), the Nyquist diagrams of the transfer functions (21) are separately depicted assuming the step response and exerting the appropriate values to the coefficients. By noticing this figure, it can be realized that the step response of load power error-based transfer function makes the angular frequency error unstable, however, the error stability is not disturbed through two other transfer functions. It is worth mentioning that the step response of transfer function $H_{tie,i}$ is able to aggrandize the stability margin of the angular frequency error accordingly. The step response-based Nyquist diagram of sum transfer functions in (20) is illustrated in Fig. 4(b). It should be paid attention that however the angular frequency error response is placed within a stable area, but the value of this error must be decreased by selecting more suitable coefficients.

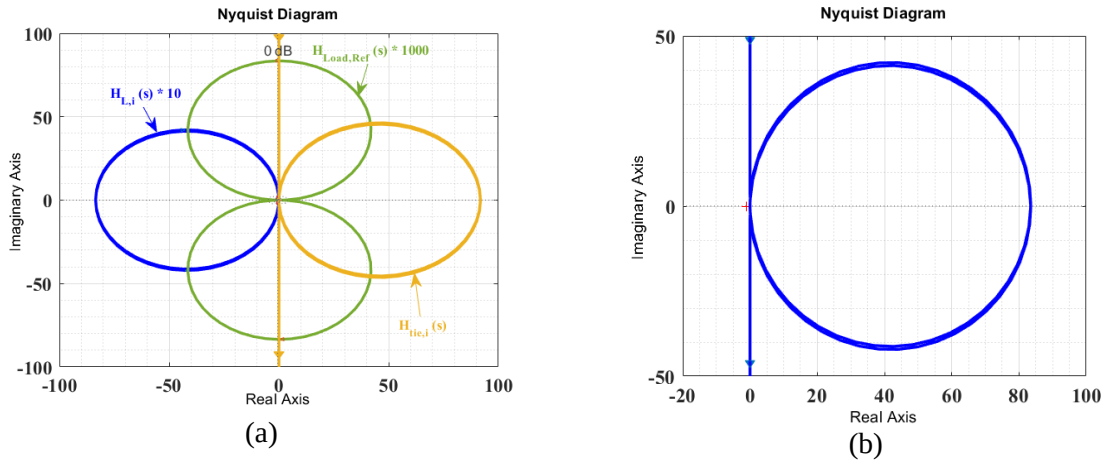

(a) (b)

Fig. 4: The step response-based Nyquist diagrams of (a) each transfer function in (21), and (b) transfer function (20).

Simulation results

In this section, MATLAB/SIMULINK software is used to assay the proposed strategy performance for making the WPG voltage stable in presence of load/PV increment at t=0.8*60 s.
The EV rated power in the related EV charging stations are within the interval [80 kW, 95 kW]. Also, the simulation is executed in 1.6 min equalizing to 96 s. The inductance X_{line} is equalized to 0.002π. As it can be seen from Fig. 5, the arrival time of all EV is zero (the beginning of the simulation). According to this figure, the departure time of most EVs is the end of simulation excepted for some of them in which the departure times are 0.7 min, 1.1 min, 0.3 min, 0.55 min, 0.75 min, 0.4 min, 1.2 min, 0.75 min, and 1.3 min.

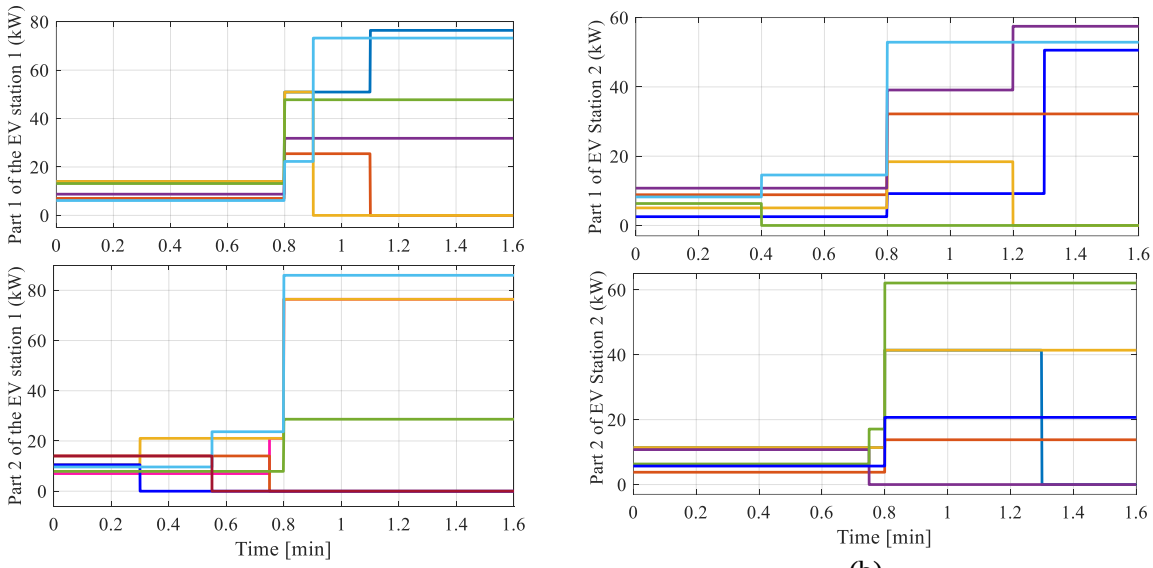

(a) (b)

Fig. 5: The instantaneous EV power injected into the WPG from, (a) the first EV charging station, and (b) the second EV charging station.

The instantaneous EV power injected into the WPG from the first and second EV charging stations are presented in Fig. 5(a) and Fig.5(b), respectively. In fact, the appropriate operation of proposed strategy leads to the EV power of the EV charging stations illustrated in these figures wherein they also result in the WPG frequency and voltage magnitude responses given in the first part of Fig. 6(a) and (b). Fig. 6 exhibits the desirable response and inappropriate responses due to mistake at the proposed strategy coefficients selection for WPG frequency, and WPG voltage magnitude. When the proposed strategy coefficients are wrongly chosen including the coefficients $\{\alpha, \beta_x, \beta_y\}$ for the power balancing and the coefficients $\{M_i, D_i, T_{m,i}, R_i, K_i, \mu_i\}$ for AGC, two unacceptable responses for both WPG frequency and WPG voltage magnitude are obtained, as depicted in the second part of Fig. 6(a) and Fig. 6(b).

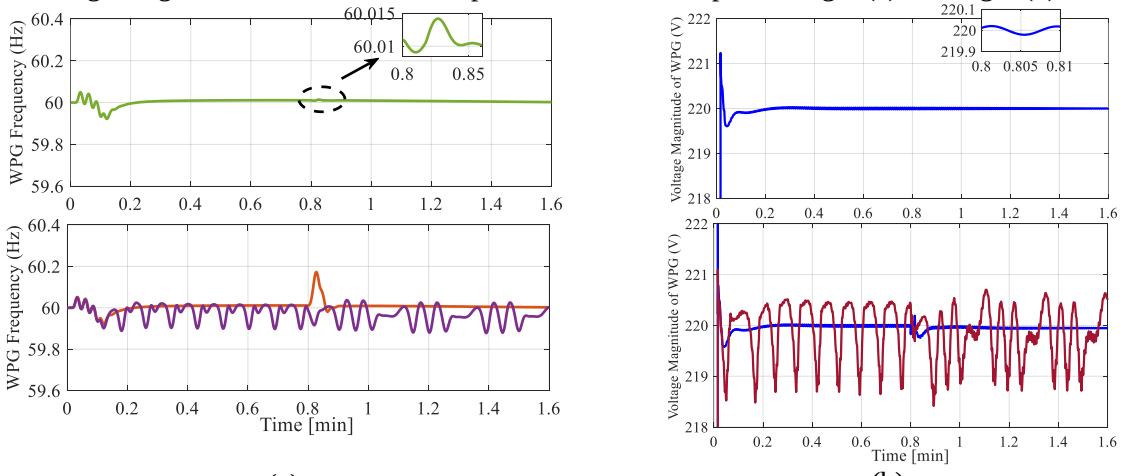

(a) (b)

Fig. 6: The desirable response and inappropriate responses due to mistake at the proposed strategy coefficients selection for (a) WPG frequency, and (b) WPG voltage magnitude.

Conclusion

This paper has presented a charging/discharging strategy for EV fleets based on automatic generation control (AGC) to provide stable voltage for WPG in presence of load/PV increment. Using the EVs specifications, the EV station power has been specified for allotting to a proposed balancing power aimed at damping the steady-state frequency error of WPG. The proposed AGC method has been designed using the angular frequency error calculation for each area and the tie-line power error along with the suitable EV action based on the proposed balancing power to significantly mitigate the dynamic change of the WPG frequency. By assessing the variations of the proposed control coefficients, the efficient coefficients have been traced to see the stability margin trend of the angular frequency error. The proposed charging/discharging strategy correctness has been approved using simulation results in MATLAB/SIMULINK environment wherein the WPG frequency and voltage magnitude could be kept stable under the PV/load increment.

References

[1] R. Razi, K. Hajar, M. Mehrasa, A. Labonne, A. Hably and S. Bacha, "Limiting discharge cycles numbers for plug-in electric vehicles in bidirectional smart charging algorithm," IECON 2021 – 47th Annual Conference of the IEEE Industrial Electronics Society, 2021, pp. 1-6.

[2] M. Mehrasa, R. Razi, K. Hajar, A. Labonne, A. Hably and S. Bacha, "Power Management of a Smart Vehicle-to-Grid (V2G) System Using Fuzzy Logic Approach," IECON 2021 – 47th Annual Conference of the IEEE Industrial Electronics Society, 2021, pp. 1-6.

[3] A. Ovalle, A. Hably, S. Bacha, "Grid Optimal Integration of Electric Vehicles: Examples with Matlab Implementation," Springer International Publishing, 2018, pp. 1-213.

[4] H. Turker and S. Bacha, "Optimal Minimization of Plug-In Electric Vehicle Charging Cost with Vehicle-to-Home and Vehicle-to-Grid Concepts," IEEE Trans. Vehicular Technology, vol. 67, no. 11, pp. 10281-10292, Nov. 2018.

[5] M. Gholami, M. Mehrasa, R. Razi, A. Hably, S. Bacha and A. Labbone, "An Efficient Control Strategy for the Hybrid Wind-Battery System to Improve Battery Performance and Lifetime," IECON2021 – 47th Annual Conference of the IEEE Industrial Electronics Society, 2021, pp. 1-6.

[6] M. Mehrasa, E. Pouresmaeil, A. Sepehr, B. Pournazarian, and J. P. S. Catalão, "Control of power electronics-based synchronous generator for the integration of renewable energies into the power grid," International Journal of Electrical Power & Energy Systems, vol. 111, pp. 300-314, Oct 2019.

[7] Y. T. Holari, S. A. Taher, and M. Mehrasa, "Distributed energy storage system-based nonlinear control strategy for hybrid microgrid power management included wind/PV units in grid-connected operation," International Transactions on Electrical Energy Systems, vol. 30, no. 2, e12237, Feb 2020.

[8] R Razi, M Mehrasa, K Hajar, M Gholami, A Hably, S Bacha, and A Labonne, "Predictive smart charging of plug-in electric vehicles for parking fleet scenario with modular converters," CIRED Porto Workshop 2022 E-mobility and power distribution systems.

[9] M. Mehrasa, R. Razi, M. Gholami, K.Hajar, A. Labonne, A. Hably, and S. Bacha, "A Dynamic Real-Time Optimization Algorithm for the Revenue Assessment of a Vehicle-To-Grid System in Presence of Wear Cost Model," Electrimacs 2022: 14th International Conference of TC-Electrimacs Committee, 16-19 May 2022 Nancy (France).

[10] K.Hajar, R. Razi, M. Mehrasa, A. Labonne, A. Hably, and S. Bacha, "Photovoltaics at the electric mobility's service: French case study," Electrimacs 2022: 14th International Conference of TC-Electrimacs Committee, 16-19 May 2022 Nancy (France).

[11] K. Hajar, B. Guo, A. Hably and S. Bacha, "Smart charging impact on electric vehicles in presence of photovoltaics," 2021 22nd IEEE International Conference on Industrial Technology (ICIT), 2021, pp. 643-648.

[12] R. Razi, K. Hajar, A. Hably and S. Bacha, "A user-friendly smart charging algorithm based on energy-awareness for different PEV parking scenarios," 2021 29th Mediterranean Conference on Control and Automation (MED), 2021, pp. 392-397.

[13] M. F. M. Arani, Y. A. I. Mohamed and E. F. El-Saadany, "Analysis and Mitigation of the Impacts of Asymmetrical Virtual Inertia," IEEE Transactions on Power Systems, vol. 29, no. 6, pp. 2862-2874, Nov. 2014.

[14] S. Flahati, S. A. Taher and M. Shahidehpour, "Grid Secondary Frequency Control by Optimized Fuzzy Control of Electric Vehicles," IEEE Transactions on Smart Grid, vol. 9, no. 6, pp. 5613-5621, Nov. 2018.

[15] K. Kaur, N. Kumar and M. Singh, "Coordinated Power Control of Electric Vehicles for Grid Frequency Support: MILP-Based Hierarchical Control Design," IEEE Transactions on Smart Grid, vol. 10, no. 3, pp. 3364-3373, May 2019.

[16] K. Kaur, M. Singh and N. Kumar, "Multiobjective Optimization for Frequency Support Using Electric Vehicles: An Aggregator-Based Hierarchical Control Mechanism," IEEE Systems Journal, vol. 13, no. 1, pp. 771-782, March 2019.
[17] C. Dong, Q. Xiao, M. Wang, T. Morstyn, M. D. McCulloch and H. Jia, "Distorted Stability Space and Instability Triggering Mechanism of EV Aggregation Delays in the Secondary Frequency Regulation of Electrical Grid-Electric Vehicle System," IEEE Transactions on Smart Grid, vol. 11, no. 6, pp. 5084-5098, Nov. 2020.
[18] S. Iqbal et al., "Aggregation of EVs for Primary Frequency Control of an Industrial Microgrid by Implementing Grid Regulation & Charger Controller," IEEE Access, vol. 8, pp. 141977-141989, 2020.
[19] M. Fakhari Moghaddam Arani and Y. A. I. Mohamed, "Cooperative Control of Wind Power Generator and Electric Vehicles for Microgrid Primary Frequency Regulation," IEEE Transactions on Smart Grid, vol. 9, no. 6, pp. 5677-5686, Nov. 2018.
[20] H. Liu, J. Qi, J. Wang, P. Li, C. Li and H. Wei, "EV Dispatch Control for Supplementary Frequency Regulation Considering the Expectation of EV Owners," IEEE Transactions on Smart Grid, vol. 9, no. 4, pp. 3763-3772, July 2018.
[21] H. Liu, Z. Hu, Y. Song, J. Wang and X. Xie, "Vehicle-to-Grid Control for Supplementary Frequency Regulation Considering Charging Demands," IEEE Transactions on Power Systems, vol. 30, no. 6, pp. 3110-3119, Nov. 2015.
[22] T. N. Pham, S. Nahavandi, L. V. Hien, H. Trinh and K. P. Wong, "Static Output Feedback Frequency Stabilization of Time-Delay Power Systems with Coordinated Electric Vehicles State of Charge Control," IEEE Transactions on Power Systems, vol. 32, no. 5, pp. 3862-3874, Sept. 2017.
[23] P. M. Rocha Almeida, J. P. Iria, F. Soares and J. A. P. Lopes, "Electric vehicles in automatic generation control for systems with large integration of renewables," 2017 IEEE Power & Energy Society General Meeting, 2017.
[24] C. Battistelli, and A. J. Conejo, "Optimal management of the automatic generation control service in smart user grids including electric vehicles and distributed resources," Electric Power Systems Research, vol. 111, pp. 22-31, June 2014.
[25] G. Wenzel, M. Negrete-Pincetic, D. E. Olivares, J. MacDonald and D. S. Callaway, "Real-Time Charging Strategies for an Electric Vehicle Aggregator to Provide Ancillary Services," IEEE Transactions on Smart Grid, vol. 9, no. 5, pp. 5141-5151, Sept. 2018.
[26] X. S. Zhang, T. Yu, Z. N. Pan, B. Yang and T. Bao, "Lifelong Learning for Complementary Generation Control of Interconnected Power Grids with High-Penetration Renewables and EVs," IEEE Transactions on Power Systems, vol. 33, no. 4, pp. 4097-4110, July 2018.
[27] E. Yao, V. W. S. Wong and R. Schober, "Robust Frequency Regulation Capacity Scheduling Algorithm for Electric Vehicles," IEEE Transactions on Smart Grid, vol. 8, no. 2, pp. 984-997, March 2017.
[28] L. Xi, L. Zhou, Y. Xu and X. Chen, "A Multi-Step Unified Reinforcement Learning Method for Automatic Generation Control in Multi-Area Interconnected Power Grid," IEEE Transactions on Sustainable Energy, vol. 12, no. 2, pp. 1406-1415, April 2021.